
Training Set Reconstruction from Differentially Private Forests: How Effective is DP?

Alice Gorgé

École Polytechnique, Palaiseau
alice.gorge@polytechnique.edu

Julien Ferry

Polytechnique Montréal
julien.ferry@polymtl.ca

Sébastien Gams

Université du Québec à Montréal
gams.sebastien@uqam.ca

Thibaut Vidal

Polytechnique Montréal
thibaut.vidal@polymtl.ca

Abstract

Recent research has shown that machine learning models are vulnerable to privacy attacks targeting their training data. To mitigate these risks, differential privacy (DP) has become a widely adopted countermeasure, as it offers rigorous privacy protection. In this paper, we introduce a reconstruction attack targeting state-of-the-art ϵ -DP random forests. By leveraging a constraint programming model that incorporates knowledge of the forest’s structure and DP mechanism characteristics, our approach formally reconstructs the *most likely* dataset that could have produced a given forest. Through extensive computational experiments, we examine the interplay between model utility, privacy guarantees and reconstruction accuracy across various configurations. Our results reveal that random forests trained with meaningful DP guarantees can still leak portions of their training data. Specifically, while DP reduces the success of reconstruction attacks, the only forests fully robust to our attack exhibit predictive performance no better than a constant classifier. Building on these insights, we provide practical recommendations for the construction of DP random forests that are more resilient to reconstruction attacks and maintain non-trivial predictive performance.

1 Introduction

The success of machine learning algorithms in critical applications, such as medicine, kidney attribution and credit scoring [Dildar et al., 2021, Aziz et al., 2021, Dastile et al., 2020], hinges on access to large volumes of sensitive data, including medical records, personal histories and financial information. This extensive data is crucial for training models capable of achieving high accuracy. At the same time, trustworthiness in these applications demands transparency, as emphasized by regulations like Article 13 of the EU AI Act¹. Transparency involves the ability to audit models and explain their outputs and inner workings, which fosters public confidence and ensures compliance with legal requirements.

However, transparency can inadvertently create vulnerabilities. When models are made public, even via black-box APIs, they become susceptible to privacy attacks that can infer sensitive information about their training data [Rigaki and Garcia, 2023]. Recent studies on reconstruction attacks [Dwork et al., 2017] demonstrated that large language models [Carlini et al., 2021], diffusion models [Carlini et al., 2023], neural networks [Haim et al., 2022], random forests (RFs) and a wide range of interpretable models [Ferry et al., 2024a,b] inherently leak part of their training data through their structure or outputs.

¹<https://artificialintelligenceact.eu/article/13/>

To mitigate such privacy risks, *differential privacy* (DP) [Dwork and Roth, 2014] has emerged as the *de facto* standard, as it limits the amount of information an adversary can gain regarding any single individual in the dataset. DP theoretically bounds the success of membership inference attacks (which aim at inferring the absence or presence of a given individual in a model’s training data), but also empirically provides a form of protection against other attacks. For instance, recent work on deep learning for medical imaging [Ziller et al., 2024] has shown that DP mitigates the success of some reconstruction attacks, even for loose privacy guarantees. However, DP imposes significant trade-offs as ensuring privacy involves adding noise or other modifications that degrade a model’s predictive performance. Consequently, practitioners must carefully balance privacy guarantees and model utility in sensitive domains.

In this paper, we focus on reconstruction attacks targeting tree ensembles, such as RFs. These models frequently achieve state-of-the-art performance on tabular data, but recent research [Ferry et al., 2024b] has revealed that their structure can inherently expose their training data. While several DP tree-based models have been designed [Fletcher and Islam, 2019], it remains unclear how well DP can effectively prevent such privacy leaks. To address this gap, the main contributions of our study are:

- We introduce an effective reconstruction attack against state-of-the-art DP RFs. Building on the attack paradigm pioneered by [Ferry et al., 2024b], our approach frames the reconstruction attack as a Constraint Programming (CP) model, which identifies a *most likely* dataset capable of generating the observed RF and noisy counts.
- Through extensive experiments, we show that DP RFs, while formally satisfying privacy guarantees, can still be exploited to retrieve portions of their training data. In particular, all investigated DP RFs with non-trivial predictive performance reveal information about their training data, which often extends beyond distributional patterns to specificities of the dataset used. To enable the reproducibility of all the experiments, the source code of our method is openly available at <https://github.com/vidalt/DRAFT-DP>, under a MIT license.
- We provide key insights regarding the factors influencing the trade-offs between DP RFs’ predictive performance and their vulnerability to reconstruction attacks. These insights aim to guide practitioners in effectively deploying DP RFs in real-world scenarios.

2 Technical Background

2.1 Differential Privacy

Originally formalized in Dwork [2006], DP enables the computation of useful statistics on private data while strictly limiting the information that can be inferred about any single individual. A randomized mechanism \mathcal{K} satisfies ϵ -DP if, for any pair of datasets D_1 and D_2 differing by at most one record, and all $U \subseteq \text{Range}(\mathcal{K})$:

$$\mathbb{P}(\mathcal{K}(D_1) \in U) \leq e^\epsilon \times \mathbb{P}(\mathcal{K}(D_2) \in U).$$

The parameter ϵ , called the privacy budget, quantifies the trade-off between privacy and utility. Smaller values of ϵ ensure stronger privacy at the expense of reduced utility.

Let q represent a deterministic query such as counts, sums, averages, or, in the context of tree ensembles, the number of samples of a particular class in a data subset. DP can give protected access to this query through a probabilistic mechanism \mathcal{K} , which outputs q with additional noise. As detailed in Dwork et al. [2016], the amount of noise needed to protect the data depends on the *global sensitivity* of the query, defined as $S(q) = \max \|q(D_1) - q(D_2)\|_1$, in which the maximum is taken over all pairs of datasets D_1 and D_2 differing in at most one element. Thus, $S(q)$ quantifies the largest possible change in the query output due to a single record’s addition or removal (e.g., $S(q) = 1$ for counts). For instance, the Laplace mechanism, a widely used DP method, adds noise sampled from a Laplace distribution:

$$\mathcal{K}(D) = q(D) + (Y_1, \dots, Y_k),$$

in which Y_i are random variables i.i.d. following the Laplace distribution $\text{Lap}(S(q)/\epsilon)$ with ϵ the privacy budget granted to the mechanism.

When multiple DP mechanisms are combined, the overall privacy budget is governed by two fundamental composition theorems [McSherry and Talwar, 2007]. First, *sequential composition* states that applying several ε_i -DP mechanisms to the same dataset results in $\sum_i \varepsilon_i$ -DP. In contrast, *parallel composition* states that applying several ε_i -DP mechanisms to disjoint subsets of data results in $\max_i \varepsilon_i$ -DP. Finally, the *postprocessing property* ensures that any function applied to the output of \mathcal{K} does not affect the DP guarantee, providing flexibility for downstream analysis.

DP mechanisms have been widely adopted to protect privacy when releasing machine learning models. For example, noise can be added to gradients during neural network training [Abadi et al., 2016], or split thresholds can be perturbed in decision tree predictors [Fletcher and Islam, 2019]. In particular, DP can mitigate privacy risks such as membership inference or model inversion [Ye et al., 2022], and implementations of DP mechanisms have been integrated within popular libraries, such as IBM’s `diffprivlib` [Holohan et al., 2019] or Google’s `differential-privacy` [Google].

2.2 Differentially-Private Random Forests

We consider a training set $D = \{\mathbf{x}_k; c_k\}_{k=1}^N$ in which each example k is characterized by a vector $\mathbf{x}_k \in \{0, 1\}^M$ of M binary attributes and a class $c_k \in \mathcal{C}$. Categorical features can be transformed into this format using one-hot encoding, as is standard practice in tree ensemble training, while continuous features can be discretized through binning. Based on this dataset, a random forest \mathcal{T} is built as an ensemble of decision trees $t \in \mathcal{T}$. Each tree consists of a set of internal nodes \mathcal{V}_t^I , in which each node $v \in \mathcal{V}_t^I$ contains a binary condition on the value of an attribute, and a set of leaves \mathcal{V}_t^L . When an example is evaluated, it traverses the tree by descending to the left child $l(v)$ if the condition is satisfied, or to the right child $r(v)$ otherwise. Once a leaf $v \in \mathcal{V}_t^L$ (terminal node) is reached, it contributes to the class distribution associated with that leaf, which is determined by the per-class counts of training examples reaching the leaf.

In most random forest implementations, including popular libraries such as `scikit-learn` [Pedregosa et al., 2011], predictions are made using *soft voting*: each tree outputs class probabilities based on the normalized class counts in its leaves and the ensemble prediction averages these probabilities. Specifically, for each leaf $v \in \mathcal{V}_t^L$ in tree t , the model stores n_{tvc} , the number of training examples of class c that reach v . This information is essential for on-device inference and audits but also introduces risks, as it exposes model parameters to potential adversaries [Ferry et al., 2024b].

To address these risks, an extensive body of research has focused on constructing DP RFs to conciliate model accessibility and privacy protection, with many of these seminal methods being surveyed by Fletcher and Islam [2019]. Among these, the method proposed by Jagannathan et al. [2012], which combines randomized tree structure and noisy counts publication, was the first to achieve strong empirical predictive performance and formal DP guarantees. Consequently, we use it as a foundation of our experimental study. In this approach, each tree is trained on the complete dataset D . Each tree of a chosen depth d is grown by randomly selecting attributes and split values for all internal nodes $v \in \mathcal{V}_t^I$, avoiding direct access to D during this phase to preserve the DP budget. Subsequently, the class counts n_{tvc} at each leaf $v \in \mathcal{V}_t^L$ are obfuscated using the Laplace mechanism [Dwork et al., 2016] and cast to integer values, as illustrated in Figure 1.

Let ε denote the total privacy budget. Since all trees $t \in \mathcal{T}$ are trained on the same dataset D , sequential composition applies, such that each tree has a budget of $\varepsilon_t = \varepsilon/|\mathcal{T}|$. Since the attributes and split values within each tree are chosen randomly without accessing the training data, the noisy computation of class counts is the sole operation consuming the DP budget. Within each tree, *parallel composition* applies since the leaves have disjoint supports. Similarly, within a leaf, the counting operations for each class are independent, also satisfying parallel composition.

Accordingly, the DP budget allocated to publish each class count n_{tvc} for $t \in \mathcal{T}, v \in \mathcal{V}_t^L, c \in \mathcal{C}$ is $\varepsilon_v = \varepsilon_t = \varepsilon/|\mathcal{T}|$. Since class counts have a global sensitivity $S(q) = 1$, the noisy class counts are computed as:

$$n_{tvc}^* = \text{int}(n_{tvc} + Y_{tvc}) = n_{tvc} + \text{int}(Y_{tvc}),$$

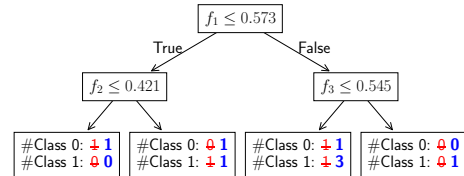


Figure 1: Example decision tree t , **before** and **after** adding Laplace noise to comply with 1-DP. The rightmost leaf, originally empty, now reports a positive sample count.

in which Y_{tvc} is a random variable sampled from a Laplace distribution $\text{Lap}(1/\varepsilon_v)$ and $\text{int}(\cdot)$ is the integer part function.

3 Reconstruction Attack against DP RFs

Attack Model. We assume *white-box* access to an ε -DP RF constructed using the algorithm of Jagannathan et al. [2012], as described in Section 2.2. This includes access to the structure of the forest (split attributes and values) and the (noisy) counts at the leaves. Consistent with the literature on reconstruction attacks [e.g., Dwork et al., 2017, Ferry et al., 2024b], we also assume knowledge of the number of attributes M and training examples N . While the knowledge of M is necessary for inference, the knowledge of N simplifies the attack but is not strictly required. In particular, in Appendix A, we demonstrate that our attack can reconstruct the dataset without prior knowledge of N , making it *the first method to target full dataset reconstruction without this assumption*. We also assume the privacy budget ε is known. This does not degrade the DP guarantees, is generally disclosed by practitioners², and researchers have advocated this for transparency [Dwork et al., 2019].

Reconstruction Approach. Our approach is grounded on the CP formulation introduced in Ferry et al. [2024b], with additional constraints, variables, and an objective specifically designed to model the (observed) noisy counts, the underlying (guessed) true counts, and their likelihood. Solving the original problem formulation (called DRAFT) was shown to be NP-Hard. Our reconstruction problem for DP RFs can be seen as a generalization (i.e., DRAFT is a special case with no noise) and is also NP-hard, though scalable with state-of-the-art CP solvers [Perron and Didier, 2024].

Our formulation revolves around three main groups of *decision variables*. The objective of a CP solver is to find compatible variable values that satisfy a given set of *constraints*, yielding a feasible solution. Moreover, as explained later in this section, an *objective function* steering the search towards likely solutions (reconstructions) will be included. First, for each tree $t \in \mathcal{T}$, the (guessed) true number of examples of class $c \in \mathcal{C}$ in each leaf $v \in \mathcal{V}_t^L$ are encoded using a variable $n_{tvc} \in \mathbb{N}$. Next, a set of variables encodes each reconstructed example $k \in \{1, \dots, N\}$: $x_{ki} \in \{0, 1\}$ encodes the value of its i^{th} attribute $i \in \{1, \dots, M\}$, while $z_{kc} \in \{0, 1\}$ indicates if it belongs to class $c \in \mathcal{C}$. Third, the path of each example $k \in \{1, \dots, N\}$ through each tree $t \in \mathcal{T}$ is modelled using a binary variable $y_{tvkc} \in \{0, 1\}$, which is 1 if it is classified by leaf $v \in \mathcal{V}_t^L$ as class $c \in \mathcal{C}$, and 0 otherwise. The following constraints linking these variables are then enforced:

$$\begin{aligned} \sum_{v \in \mathcal{V}_t^L} \sum_{c \in \mathcal{C}} n_{tvc} &= N & t \in \mathcal{T} \quad (1) \quad z_{kc} &= \sum_{v \in \mathcal{V}_t^L} y_{tvkc} & k \in \{1, \dots, N\}, t \in \mathcal{T}, c \in \mathcal{C} \quad (3) \\ \sum_{c \in \mathcal{C}} z_{kc} &= 1 & k \in \{1, \dots, N\} \quad (2) \quad \sum_{k=1}^N y_{tvkc} &= n_{tvc} & t \in \mathcal{T}, v \in \mathcal{V}_t^L, c \in \mathcal{C} \quad (4) \end{aligned}$$

In a nutshell, Constraint (1) ensures that the example counts sum up to N within each tree. Constraint (2) guarantees that each example is associated to exactly one class. Constraint (3) enforces that each example contributes only to the counts of its assigned class. Moreover, Constraint (4) ensures consistency between the counts at each leaf and the examples assigned to it. Finally, for each leaf $v \in \mathcal{V}_t^L$ of each tree $t \in \mathcal{T}$, let Φ_v^+ (respectively Φ_v^-) be the set of binary attributes that must equal 1 (respectively 0) for an example to fall into v . Then, the following constraint enforces consistency between the examples' assignments to the leaves, and the value of their attributes:

$$\sum_{c \in \mathcal{C}} y_{tvkc} = 1 \Rightarrow \left(\bigwedge_{i \in \Phi_v^+} x_{ki} = 1 \right) \wedge \left(\bigwedge_{i \in \Phi_v^-} x_{ki} = 0 \right) \quad t \in \mathcal{T}, v \in \mathcal{V}_t^L, k \in \{1, \dots, N\} \quad (5)$$

Optionally, if additional structural knowledge about the features is available, e.g., one-hot encoding or logical/linear relationships between their values, this information can be incorporated by adding the corresponding constraints on the x_{ki} values for each sample k .

The aforementioned variables and constraints define the **domain of all possible datasets and associated counts n_{tvc} compatible with the structure and split values of an observed forest**. Among all solutions in this domain, we aim at retrieving the one that is the *most likely* to have

²For example, Desfontaines [2021] documents real-world applications of DP and their associated budgets.

generated the observed noisy counts n_{tvc}^* through the DP mechanism. To this end, we formulate through Constraint (6) the noise Δ_{tvc} that must have been added to each count to achieve the observed values.

$$\Delta_{tvc} = n_{tvc}^* - n_{tvc} \quad t \in \mathcal{T}, v \in \mathcal{V}_t^L, c \in \mathcal{C} \quad (6)$$

We know that these noise values correspond to i.i.d realizations of random variables Y_{tvc} from a Laplace distribution $\text{Lap}(1/\varepsilon_v)$ cast to integer. Given this information, the *likelihood* of a complete solution associated to a set of Δ_{tvc} values is defined in Equation (7). Maximizing this likelihood is equivalent to maximizing its logarithm, leading to the objective function in Equation (8).

$$\mathcal{P}_\Delta = \prod_{t,v,c} \mathbb{P}(\text{int}(Y_{tvc}) = \Delta_{tvc}) \quad (7) \quad \max \log(\mathcal{P}_\Delta) = \sum_{t,v,c} \log(\mathbb{P}(\text{int}(Y_{tvc}) = \Delta_{tvc})) \quad (8)$$

The Laplace distribution density with parameter $(1/\varepsilon_v)$ is given by $\mathcal{L}(u) = \frac{\varepsilon_v}{2} e^{-|u|\varepsilon_v}$. Since the noisy counts are cast to integer values, the probability of a specific (integer) noise value l is:

$$p_l = \mathbb{P}(\text{int}(Y_{tvc}) = l) = \begin{cases} \int_l^{l+1} \frac{\varepsilon_v}{2} e^{-|u|\varepsilon_v} du & \text{if } l > 0, \\ \int_{-1}^1 \frac{\varepsilon_v}{2} e^{-|u|\varepsilon_v} du & \text{if } l = 0, \\ \int_{l-1}^l \frac{\varepsilon_v}{2} e^{-|u|\varepsilon_v} du & \text{if } l < 0. \end{cases}$$

In practice, we pre-compute constants p_l for all values $l \in \{-\delta, \dots, \delta\}$ such that $\mathbb{P}(\text{int}(Y_{tvc}) \in \{-\delta, \dots, \delta\}) \geq 0.999$. Details on the computation of δ are provided in Appendix B, but typically, $\delta = \lceil 12/\varepsilon_v \rceil$ is sufficient. With this, we can additionally restrict the feasible domain of the variables to $n_{tvc} \in \{\max(0, n_{tvc}^* - \delta), \dots, n_{tvc}^* + \delta\}$ and $\Delta_{tvc} \in \{-\delta, \dots, \delta\}$ and formulate the objective as:

$$\max \sum_{t \in \mathcal{T}} \sum_{v \in \mathcal{V}_t^L} \sum_{c \in \mathcal{C}} \sum_{l=-\delta}^{\delta} \log(p_l) \mathbb{1}_{\Delta_{tvc}=l}, \quad (9)$$

in which the indicator $\mathbb{1}_{\Delta_{tvc}=l}$ can efficiently be expressed in CP using *domain mapping* constraints based on the values of the Δ_{tvc} variables.

4 Experimental Study

We now empirically evaluate our proposed reconstruction attack, and investigate whether it succeeds in accurately inferring a RF training data despite the DP protection. The source code and data needed to reproduce all our experiments and figures are available at <https://github.com/vidalr/DRAFT-DP>, under a MIT license.

4.1 Experimental Setup

Datasets and target models. We rely on three datasets, using the same data preprocessing as in Ferry et al. [2024b]. The COMPAS dataset [Angwin et al., 2016] contains records of 7,206 criminal offenders from Florida, each characterized by 15 binary attributes, and is used for recidivism prediction. The UCI Adult Income dataset [Dua and Graff, 2017] gathers data on 48,842 individuals from the 1994 U.S. census. Each individual is described by 20 binary features, with the objective of predicting whether an individual earns more than \$50K/year. Finally, the Default of Credit Card Clients (Default Credit) dataset [Yeh and hui Lien, 2009] includes 29,986 customer records from Taiwan, with 22 binary attributes, to predict payment defaults.

The ε -DP RFs are trained as described in Section 2.2. In practice, we build upon the efficient and modular implementation of IBM’s `diffprivlib` library [Holohan et al., 2019], which we slightly adapt for our experiments. Following Ferry et al. [2024b], each experiment uses a randomly sampled training set of $N = 100$ examples. While this sample size is in line with the literature and allows all experiments to be conducted in a moderate time frame, we also report results with larger training datasets in Appendix E, demonstrating the scalability of the approach. We build DP RFs of size $|\mathcal{T}| \in \{1, 5, 10, 20, 30\}$ and of maximum depth $d \in \{3, 5, 7\}$. Empirical evidence from Fan et al. [2003] suggests that the predictive accuracy of a random forest typically plateaus beyond 30 trees, with 10 to 30 trees being sufficient for robust performance. This is particularly true in the DP setting,

in which adding trees consumes additional privacy budget [Fletcher and Islam, 2019]. Finally, we evaluate privacy parameters $\varepsilon \in \{0.1, 1, 5, 10, 20, 30\}$, ranging from very tight to large privacy budgets, which reflect commonly used values in practice [Desfontaines, 2021].

Reconstruction attack. We use the `OR-Tools` CP-SAT solver [Perron and Didier, 2024] (v9) to solve the CP formulation introduced in Section 3. Each model resolution is limited to a maximum of 2 hours of CPU time using 16 threads with up to 7 GB of RAM per thread. Note that in practice, feasible solutions – i.e., reconstructions that are compatible with the RF’s structure and the observed noisy counts – can be obtained using only a small fraction of the 2-hours timeout (in average, less than two minutes), as reported in Appendix C.1. All experiments are run on a computing cluster over a set of homogeneous nodes with AMD EPYC 7532 (Zen 2) @ 2.40 GHz CPU.

We consider two baselines in our experiments. As in Ferry et al. [2024b], a random reconstruction baseline is used to quantify the amount of information that can be inferred without knowledge of the RF (i.e., only based on the number of examples N , the different attributes M , their domains and one-hot encoding). This baseline randomly guesses the value of each attribute of each example while remaining consistent with one-hot encoding when applicable (we average its performance over 100 runs). To quantify the effect of DP on the reconstruction error, we also run the state-of-the-art DRAFT attack against the trained RFs without the DP protection (i.e., with the true leaves’ counts).

In line with the literature [Ferry et al., 2024b], while a reconstructed dataset is inferred, first it is aligned with the original training set using a minimum cost matching with the Manhattan distance, in order to identify which reconstructed examples correspond to which original ones. Then, the proportion of binary attributes that differ is averaged over the entire dataset to quantify the reconstruction error. Each experiment is repeated using five different random seeds and the results are averaged.

4.2 Results

Result 1. Reconstruction attacks succeed against DP RFs, even with meaningful privacy guarantees. Table 1 reports the reconstruction error for all our experiments. For commonly protective privacy budgets (e.g., $\varepsilon = 1$ or 5), our attack achieves significantly lower reconstruction error compared to the random baseline. This indicates that the adversary was able to gain insights from the RF to better infer the training data. Nonetheless, the reconstruction error consistently increases when reducing the privacy budget ε , which suggests that DP partially mitigates the reconstruction success. To assess this, Figure 2 compares the effectiveness of our reconstruction to that of DRAFT [Ferry et al., 2024b] applied on the same RF (without DP). For very tight privacy budgets (e.g., small ε), DP significantly increases the reconstruction error compared to the DRAFT baseline. However, as ε increases, the protective effect of DP diminishes, and the difference in reconstruction error between our attack and DRAFT becomes much smaller, even for ε values commonly considered protective.

Result 2. DP leads to a complex trade-off between the RFs’ size and the reconstruction attack success. As can be seen in Figure 2, larger DP RFs do not necessarily provide more information to the attacker, unlike non-DP RFs. A threshold effect is observed: the reconstruction error decreases as the number of trees increases, up to a point (typically around 5-10 trees), before increasing again. This behavior is consistent across all privacy budgets and is likely due to the privacy budget being distributed across more trees, resulting in noisier counts for individual leaves. Similarly, while deeper trees in the non-DP setting provide more information to the attacker, this is not always the case for DP RFs (see also, Table 1) since smaller leaves’ counts are proportionally more affected by the noise.

Result 3. Protection against reconstruction attacks comes at the expense of predictive accuracy. As shown in Table 1, the considered DP mechanism effectively mitigates the success of reconstruction attacks at very low ε values (e.g., $\varepsilon = 0.1$). However, at these privacy levels, the resulting RFs have poor predictive accuracy, often performing no better than a majority prediction classifier, as illustrated in Figure 3. Notably, only RFs with trivial predictive performance provide no advantage to the reconstruction adversary (compared to the random reconstruction baseline). This is also visible in Figure 4, in which most RFs either perform better than a majority classifier but provide a significant advantage to the reconstruction attacker (upper left corner), or provide no advantage to the attacker but perform worse than a majority classifier (lower right corner).

Result 4. For typical values of ε , one can infer information specific to the DP RF training set beyond general distributional patterns. The results in Table 1 demonstrate that the proposed attack extracts information useful for accurately reconstructing the DP RF training dataset D , which

Table 1: Average reconstruction error for different numbers of trees $|\mathcal{T}|$, tree depths d and privacy budgets ϵ for the three datasets. Reconstruction errors worse than the random baseline are **bold**. Cases where the solver failed to find a feasible reconstruction within the time limit are marked with “-”.

	Adult			COMPAS			Default Credit			
	$d=3$	$d=5$	$d=7$	$d=3$	$d=5$	$d=7$	$d=3$	$d=5$	$d=7$	
$ \mathcal{T} = 1$	$\epsilon = 0.1$	0.26	0.24	0.22	0.29	0.28	0.21	0.35	0.31	0.29
	$\epsilon = 1$	0.25	0.20	0.17	0.26	0.20	0.14	0.32	0.29	0.24
	$\epsilon = 5$	0.24	0.23	0.30	0.25	0.20	0.18	0.32	0.31	0.25
	$\epsilon = 10$	0.24	0.22	0.33	0.25	0.21	0.18	0.32	0.30	0.27
	$\epsilon = 20$	0.24	0.19	0.27	0.25	0.17	0.20	0.32	0.28	0.30
	$\epsilon = 30$	0.24	0.19	0.27	0.25	0.16	0.18	0.32	0.29	0.31
$ \mathcal{T} = 5$	$\epsilon = 0.1$	0.26	0.24	0.24	0.23	0.24	0.23	0.32	0.27	0.29
	$\epsilon = 1$	0.19	0.18	0.20	0.14	0.13	0.12	0.23	0.23	0.22
	$\epsilon = 5$	0.17	0.14	0.11	0.10	0.07	0.05	0.22	0.16	0.15
	$\epsilon = 10$	0.17	0.13	0.10	0.10	0.06	0.04	0.22	0.16	0.13
	$\epsilon = 20$	0.16	0.12	0.08	0.09	0.05	0.02	0.21	0.15	0.11
	$\epsilon = 30$	0.16	0.13	0.09	0.10	0.05	0.03	0.21	0.16	0.11
$ \mathcal{T} = 10$	$\epsilon = 0.1$	0.28	0.31	0.34	0.25	0.28	0.28	0.32	0.31	0.30
	$\epsilon = 1$	0.17	0.19	0.23	0.12	0.14	0.16	0.21	0.24	0.24
	$\epsilon = 5$	0.15	0.12	0.15	0.07	0.07	0.06	0.15	0.16	0.19
	$\epsilon = 10$	0.13	0.10	0.11	0.06	0.05	0.04	0.14	0.13	0.13
	$\epsilon = 20$	0.14	0.09	0.09	0.06	0.03	0.03	0.14	0.12	0.11
	$\epsilon = 30$	0.13	0.08	0.09	0.05	0.03	0.02	0.14	0.11	0.09
$ \mathcal{T} = 20$	$\epsilon = 0.1$	0.28	0.34	0.30	0.29	0.34	0.33	0.29	0.35	0.33
	$\epsilon = 1$	0.19	0.22	0.22	0.16	0.19	0.19	0.23	0.25	0.26
	$\epsilon = 5$	0.12	0.16	0.19	0.09	0.08	0.14	0.17	0.19	0.21
	$\epsilon = 10$	0.11	0.11	0.14	0.06	0.06	0.10	0.14	0.14	0.18
	$\epsilon = 20$	0.11	0.09	0.10	0.05	0.05	0.05	0.12	0.12	0.13
	$\epsilon = 30$	0.10	0.09	0.08	0.04	0.03	0.04	0.12	0.11	0.12
$ \mathcal{T} = 30$	$\epsilon = 0.1$	0.34	0.35	-	0.33	0.33	-	0.36	0.38	-
	$\epsilon = 1$	0.21	0.22	0.25	0.17	0.20	0.21	0.23	0.26	0.25
	$\epsilon = 5$	0.15	0.16	0.22	0.09	0.10	0.16	0.17	0.20	0.24
	$\epsilon = 10$	0.13	0.14	0.18	0.07	0.08	0.13	0.14	0.14	0.19
	$\epsilon = 20$	0.10	0.10	0.13	0.06	0.06	0.09	0.13	0.13	0.17
	$\epsilon = 30$	0.10	0.09	0.11	0.04	0.04	0.06	0.11	0.11	0.13
Random baseline	0.25			0.21			0.26			

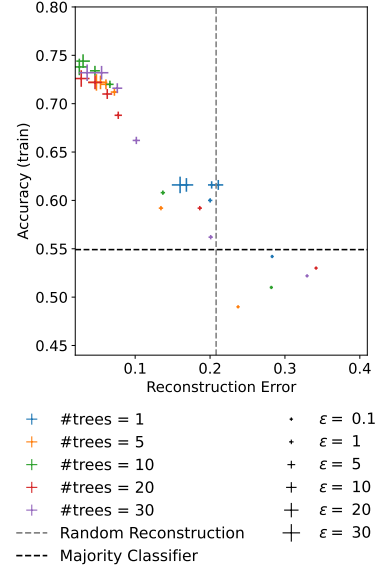


Figure 4: Average training accuracy of ϵ -DP RFs with depth-5 trees as a function of the reconstruction error, for different privacy budgets ϵ and forest sizes $|\mathcal{T}|$ on the COMPAS dataset.

may reflect general distributional patterns and/or dataset-specific details. While the former is still valuable—especially given that our attack assumes no knowledge of the data distribution—privacy leakages are typically defined in terms of recovering information specific to the actual training set [Cohen et al., 2025]. Appendix D presents a complementary analysis in which we assess *whether the reconstructed dataset is closer to D than to other datasets from the same data distribution, in*

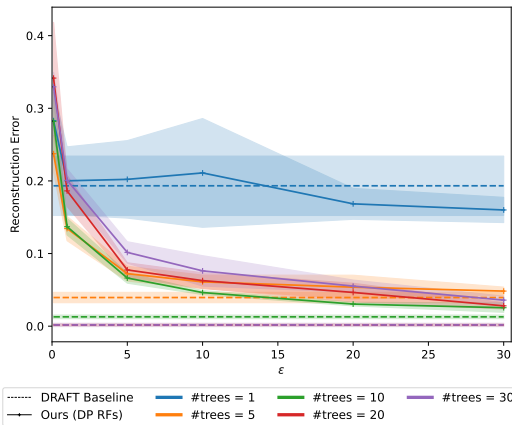


Figure 2: Average reconstruction error as a function of the privacy budget ϵ used to fit the target RF, for different numbers of depth-5 trees $|\mathcal{T}|$ on the COMPAS dataset. For comparison, we also report the reconstruction error of DRAFT applied to the same RFs without DP protection.

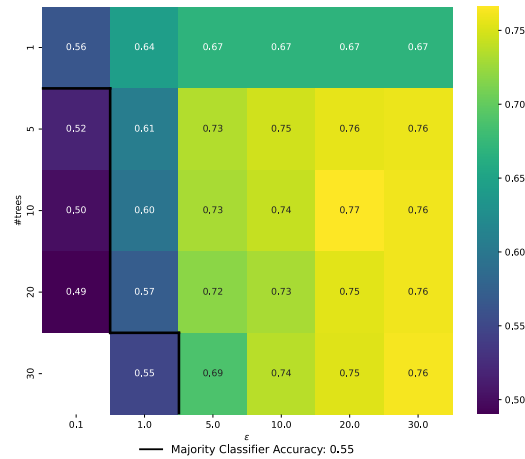


Figure 3: Average training accuracy of ϵ -DP RFs with depth-7 trees as a function of the privacy budget ϵ , for different forest sizes $|\mathcal{T}|$ on the COMPAS dataset

a statistically significant manner. The results suggest that for very tight DP budgets (i.e., $\epsilon = 0.1$), only distributional information is inferred while larger DP budgets (i.e., $\epsilon \geq 5$) usually allow the retrieval of dataset-specific details. Between these two extrema, several configurations with small DP budgets (i.e., $\epsilon = 1$) can also lead to the inference of information specific to D . This emphasizes the need to thoroughly tune all hyperparameters beyond the sole DP budget.

Result 5. Knowledge of the training set size N is unnecessary. While prior work often assumes knowledge of the training set size N , Appendix A presents a modified version of our CP model that enables reconstruction without this information. Our experiments demonstrate that accurate reconstruction remains feasible under this assumption. Although the computational cost and reconstruction error increase slightly compared to the traditional setup in which N is known, the attack remains highly effective for most practically relevant ϵ values.

Result 6. The reconstruction attack scales well with the number of training examples N . In the Appendix E, we report results of additional experiments varying the size of the reconstructed training set N . They demonstrate that increasing the number of training examples N improves the predictive performance and generalization of the built DP RFs, but also significantly benefits the reconstruction attack. For instance, the attack’s average reconstruction error against DP RFs with $|\mathcal{T}| = 10$ depth-5 trees and $\epsilon = 5$ decreases from 0.16 to 0.11 when increasing the number of training examples from the Default of Credit Card Clients dataset from $N = 100$ to $N = 500$. This is due to the fact that the relative impact of the noise added to enforce DP decreases as N increases, leading to more accurate leaf counts benefiting both the RF predictive performance and the proposed reconstruction attack.

Result 7. Knowledge of part of the training set attributes does not help reconstruct the others. In Appendix F, we report results of additional experiments assuming knowledge of part of the attributes, for all training examples. This setup corresponds to the situation in which part of the examples’ attributes are public information, and prior work on dataset reconstruction from (non-DP) RFs [Ferry et al., 2024b] demonstrated that knowing them facilitates the reconstruction of the others. We consistently observe that it is not the case when handling DP RFs: regardless of how many attributes the adversary knows, no advantage is gained to better reconstruct the remaining ones. Therefore, while DP does not entirely prevent the extraction of information useful for reconstructing the RF training dataset, it offers an interesting complementary protection by limiting the adversary’s ability to exploit auxiliary information.

5 Related Work

Reconstruction Attacks and DP. Reconstruction attacks were first introduced against database queries by Dinur and Nissim [2003]. In their setup, all database columns are public except for a binary one, which the adversary attempts to recover using (noisy) responses to counting queries. By modeling the noise within a linear programming framework, their attack successfully retrieves the private bit for all individuals. Over the following decade, several works extended this approach [Dwork et al., 2017]. More recently, reconstruction attacks have been adapted to machine learning models. Unlike database-focused ones, these attacks often aim to infer specific attributes or recover information about individual samples rather than reconstructing the entire training set [Fredrikson et al., 2015]. Many of these attacks also rely on auxiliary information beyond the trained model, such as intermediate gradients computed during training [Phong et al., 2017, Salem et al., 2020], stationary points reached during optimization [Haim et al., 2022] or fairness-related constraints [Hu and Lan, 2020, Hamman et al., 2022, Ferry et al., 2023].

In contrast, recent studies have shown that tree-based models are vulnerable to reconstruction attacks due to their combinatorial structure. For example, Gambis et al. [2012] and Ferry et al. [2024a] developed algorithms leveraging white-box access to a single decision tree to reconstruct a probabilistic representation of its dataset, encoding all reconstructions consistent with the tree’s structure. More recently, Ferry et al. [2024b] proposed DRAFT, a CP-based reconstruction attack against RFs, showing that the structure of an RF can be exploited to reconstruct most of its training data efficiently.

DP has been shown empirically to mitigate reconstruction attacks on deep neural networks [Ziller et al., 2024] and language models [Stock et al., 2022]. However, these defenses often come at a significant cost to model performance, and the considered attacks typically do not exploit the DP mechanism explicitly. Our work advances this field by (1) explicitly accounting for the DP mechanism

within the attack formulation, and (2) analyzing the trade-offs between the DP budget, the empirical reconstruction attack success and the DP model’s predictive performances in the context of tree ensembles.

Building DP Random Forests. Traditional tree induction algorithms iteratively perform a greedy selection of the attributes and values to split on at each level of the considered tree, based on some information gain criterion. Some works on DP RFs proceed similarly [Patil and Singh, 2014, Fletcher and Islam, 2015b, Rana et al., 2015]. However, since the training data needs to be accessed at each level of the tree to greedily determine the splits, the DP budget ϵ must be divided between them, resulting in the addition of a significant amount of noise. Thus, other approaches proposed to randomly determine all splitting attributes and values [Jagannathan et al., 2012, Fletcher and Islam, 2015a, 2017], and only access the data to populate the leaves. Even if random splits may partition the data imperfectly, this reduction in the amount of noise required to ensure DP generally allows for better predictive performance. Note that this specific aspect makes no difference in our attack’s design, since the reconstruction model does not directly exploit the way the splits are determined.

In non-DP RFs, bootstrap sampling (bagging) is commonly used to generate each tree’s training set, by performing sampling with replacement from N to N . While some DP RF approaches [Rana et al., 2015] have adopted this strategy, providing tight and thorough DP guarantees remains challenging, as bootstrapped subsets are not disjoint and often contain multiple occurrences of certain examples. An alternative is to divide the original dataset into disjoint subsets to independently train each tree, enabling parallel composition of the privacy budget [Fletcher and Islam, 2015a, 2017]. However, this approach may harm predictive performance as each tree is trained on significantly less data. Moreover, this also results in smaller leaves’ class counts, which in turn are proportionally more affected by the noise added to enforce DP. A standard approach is to learn all trees on the full training dataset, even though it requires dividing the privacy budget across trees [Jagannathan et al., 2012, Fletcher and Islam, 2015a, 2017, Patil and Singh, 2014, Fletcher and Islam, 2015b]. Our attack could handle bagging as in Ferry et al. [2024b]. However, if the trees are trained on disjoint subsets, a per-tree probabilistic reconstruction approach such as the one proposed by Ferry et al. [2024a] suffices, since nothing can be gained by relating the information discovered across different trees.

Finally, some approaches such as IBM’s `diffprivlib` implementation [Holohan et al., 2019], release only (noisy) majority labels within the leaves of DP RFs to conserve the privacy budget instead of providing full class counts. However, this strategy prevents the use of the traditional soft voting scheme for inference, relying instead on simple majority voting, which may degrade predictive performance. Furthermore, the access to class counts is often necessary for auditing purposes. Adapting the attack developed in this study to handle this setup would require modifying the objective function and introducing additional variables, to compute the likelihood of generating an observed (noisy) majority label for each leaf based on the guessed class counts.

6 Conclusion

This work has demonstrated that even with a low privacy budget, accurate reconstruction of the training examples of an ϵ -DP RF remains possible. Crucially, it shows that a model can comply with rigorous DP guarantees while still providing significant information regarding its training dataset to potential reconstruction attackers. This highlights that privacy protection cannot be solely reduced to choosing a sufficiently small ϵ . Rather, the design of the DP mechanism itself plays a fundamental role in mitigating reconstruction risks. This aligns with recent findings on privacy attacks (i.e., re-identification and attribute inference) against local-differentially private protocols, in which the attack success depends not only on ϵ but also on the mechanism’s structure [Arcolezi et al., 2023]. Similarly, our results suggest that a careful selection of the hyperparameters used to tune the RF and the DP mechanism allows for better trade-offs between predictive performance and empirical protection against reconstruction attacks.

The research avenues connected to this work are numerous. One first direction involves extending the proposed reconstruction framework to DP RFs trained with alternative mechanisms —e.g., adding noise from different distributions or distributing it adaptively across the different algorithm components— or revealing different information, as discussed in Section 5. Notably, we observe that any known *prior* on the dataset distribution can be embedded into the likelihood objective. Next, our approach lays the foundation for a more systematic privacy evaluation methodology grounded

on mathematical programming, which integrates available knowledge from the training model as constraints and guides the search towards a most likely solution according to the underlying DP mechanism specifications. This framework can serve as a benchmark for DP strategies, helping to analyze how different DP configurations influence the trade-off between privacy and model utility. Understanding this interplay is crucial for developing machine learning models that are not only privacy-preserving in theory but also practically usable and robust against real-world privacy attacks.

Acknowledgements

This research was enabled by support provided by Calcul Québec and the Digital Research Alliance of Canada, as well as funding from the SCALE AI Chair in Data-Driven Supply Chains.

References

- Martin Abadi, Andy Chu, Ian Goodfellow, H. Brendan McMahan, Ilya Mironov, Kunal Talwar, and Li Zhang. Deep learning with differential privacy. In *Proceedings of the 2016 ACM SIGSAC Conference on Computer and Communications Security, CCS'16*, pages 308–318. ACM, 2016.
- Julia Angwin, Jeff Larson, Surya Mattu, and Lauren Kirchner. Machine bias: There's software used across the country to predict future criminals. and it's biased against blacks. *propublica* (2016). *ProPublica*, May, 23, 2016.
- Héber Hwang Arcolezi, Sébastien Gambs, Jean-François Couchot, and Catuscia Palamidessi. On the risks of collecting multidimensional data under local differential privacy. *Proc. VLDB Endow.*, 16(5):1126–1139, 2023.
- Haris Aziz, Ágnes Cseh, John P. Dickerson, and Duncan C. McElfresh. Optimal kidney exchange with immunosuppressants. In *Proceedings of the 35th AAAI Conference on Artificial Intelligence, AAAI 2021*, pages 21–29. AAAI Press, 2021.
- Nicholas Carlini, Florian Tramèr, Eric Wallace, Matthew Jagielski, Ariel Herbert-Voss, Katherine Lee, Adam Roberts, Tom Brown, Dawn Song, Úlfar Erlingsson, Alina Oprea, and Colin Raffel. Extracting training data from large language models. In *30th USENIX Security Symposium, USENIX Security 2021*, pages 2633–2650. USENIX Association, 2021.
- Nicholas Carlini, Jamie Hayes, Milad Nasr, Matthew Jagielski, Vikash Sehwal, Florian Tramèr, Borja Balle, Daphne Ippolito, and Eric Wallace. Extracting training data from diffusion models. In *32nd USENIX Security Symposium, USENIX Security 2023*, pages 5253–5270. USENIX Association, 2023.
- Edith Cohen, Haim Kaplan, Yishay Mansour, Shay Moran, Kobbi Nissim, Uri Stemmer, and Eliad Tsfadia. Data reconstruction: When you see it and when you don't. In *16th Innovations in Theoretical Computer Science Conference, ITCS 2025*, volume 325 of *LIPIcs*, pages 39:1–39:23. Schloss Dagstuhl - Leibniz-Zentrum für Informatik, 2025.
- Xolani Dastile, Turgay Çelik, and Moshe Potsane. Statistical and machine learning models in credit scoring: A systematic literature survey. *Appl. Soft Comput.*, 91:106263, 2020.
- Damien Desfontaines. A list of real-world uses of differential privacy. <https://desfontain.es/blog/real-world-differential-privacy.html>, 10 2021. Ted is writing things (personal blog).
- Mehwish Dildar, Shumaila Akram, Muhammad Irfan, Hikmat Ullah Khan, Muhammad Ramzan, Abdur Rehman Mahmood, Soliman Ayed Alsaiari, Abdul Hakeem M Saeed, Mohammed Olaythah Alraddadi, and Mater Hussien Mahnashi. Skin cancer detection: a review using deep learning techniques. *International journal of environmental research and public health*, 18(10):5479, 2021.
- Irit Dinur and Kobbi Nissim. Revealing information while preserving privacy. In *Proceedings of the Twenty-Second ACM SIGACT-SIGMOD-SIGART Symposium on Principles of Database Systems*, pages 202–210. ACM, 2003.

- Dheeru Dua and Casey Graff. UCI machine learning repository, 2017. URL <http://archive.ics.uci.edu/ml>.
- Cynthia Dwork. Differential privacy. In *Automata, Languages and Programming*, pages 1–12. Springer Berlin Heidelberg, 2006. ISBN 978-3-540-35908-1.
- Cynthia Dwork and Aaron Roth. The algorithmic foundations of differential privacy. *Foundations and Trends® in Theoretical Computer Science*, 9(3–4):211–407, 2014. ISSN 1551-305X.
- Cynthia Dwork, Frank McSherry, Kobbi Nissim, and Adam D. Smith. Calibrating noise to sensitivity in private data analysis. *J. Priv. Confidentiality*, 7(3):17–51, 2016.
- Cynthia Dwork, Adam Smith, Thomas Steinke, and Jonathan Ullman. Exposed! a survey of attacks on private data. *Annual Review of Statistics and Its Application*, 4:61–84, 2017.
- Cynthia Dwork, Nitin Kohli, and Deirdre K. Mulligan. Differential privacy in practice: Expose your epsilons! *J. Priv. Confidentiality*, 9(2), 2019.
- Wei Fan, Haixun Wang, Philip S. Yu, and Sheng Ma. Is random model better? on its accuracy and efficiency. In *Proceedings of the 3rd IEEE International Conference on Data Mining, ICDM 2003*, pages 51–58. IEEE Computer Society, 2003.
- Julien Ferry, Ulrich Aïvodji, Sébastien Gambs, Marie-José Huguet, and Mohamed Siala. Exploiting fairness to enhance sensitive attributes reconstruction. In *First IEEE Conference on Secure and Trustworthy Machine Learning, SaTML 2023*, pages 18–41, 2023.
- Julien Ferry, Ulrich Aïvodji, Sébastien Gambs, Marie-José Huguet, and Mohamed Siala. Probabilistic dataset reconstruction from interpretable models. In *Second IEEE Conference on Secure and Trustworthy Machine Learning, SaTML 2024*, pages 1–17. IEEE, 2024a.
- Julien Ferry, Ricardo Fukasawa, Timothée Pascal, and Thibaut Vidal. Trained random forests completely reveal your dataset. In *Proceedings of the 41st International Conference on Machine Learning, ICML 2024*, volume 235 of *Proceedings of Machine Learning Research*, pages 13545–13569. PMLR, 2024b.
- Sam Fletcher and Md Zahidul Islam. A differentially private random decision forest using reliable signal-to-noise ratios. In *AI 2015: Advances in Artificial Intelligence - 28th Australasian Joint Conference*, volume 9457 of *Lecture Notes in Computer Science*, pages 192–203. Springer, 2015a.
- Sam Fletcher and Md Zahidul Islam. A differentially private decision forest. In *Thirteenth Australasian Data Mining Conference, AusDM 2015*, volume 168 of *CRPIT*, pages 99–108. Australian Computer Society, 2015b.
- Sam Fletcher and Md Zahidul Islam. Differentially private random decision forests using smooth sensitivity. *Expert Systems with Applications*, 78:16–31, 2017. ISSN 0957-4174.
- Sam Fletcher and Md Zahidul Islam. Decision tree classification with differential privacy: A survey. *ACM Comput. Surv.*, 52(4):83:1–83:33, 2019.
- Matt Fredrikson, Somesh Jha, and Thomas Ristenpart. Model inversion attacks that exploit confidence information and basic countermeasures. In *Proceedings of the 22nd ACM SIGSAC Conference on Computer and Communications Security*, pages 1322–1333. ACM, 2015.
- Sébastien Gambs, Ahmed Gmati, and Michel Hurfin. Reconstruction attack through classifier analysis. In *Data and Applications Security and Privacy XXVI - 26th Annual IFIP WG 11.3 Conference, DBSec 2012*, volume 7371 of *Lecture Notes in Computer Science*, pages 274–281. Springer, 2012.
- Google. Google’s differential privacy libraries. <https://github.com/google/differential-privacy/>.
- Niv Haim, Gal Vardi, Gilad Yehudai, Ohad Shamir, and Michal Irani. Reconstructing training data from trained neural networks. In *Advances in Neural Information Processing Systems, NeurIPS 2022*, volume 35, pages 22911–22924. Curran Associates, Inc., 2022.

- Faisal Hamman, Jiahao Chen, and Sanghamitra Dutta. Can querying for bias leak protected attributes? achieving privacy with smooth sensitivity. In *NeurIPS 2022 Workshop on Algorithmic Fairness through the Lens of Causality and Privacy*, 2022.
- Naiose Holohan, Stefano Braghin, Pól Mac Aonghusa, and Killian Levacher. Diffprivlib: The IBM differential privacy library. *CoRR*, abs/1907.02444, 2019.
- Hui Hu and Chao Lan. Inference attack and defense on the distributed private fair learning framework. In *The AAAI Workshop on Privacy-Preserving Artificial Intelligence*, 2020.
- Geetha Jagannathan, Krishnan Pillaipakkamnatt, and Rebecca N. Wright. A practical differentially private random decision tree classifier. *Trans. Data Priv.*, 5(1):273–295, 2012.
- Frank McSherry and Kunal Talwar. Mechanism design via differential privacy. In *48th Annual IEEE Symposium on Foundations of Computer Science (FOCS 2007)*, pages 94–103. IEEE Computer Society, 2007.
- Abhijit Patil and Sanjay Singh. Differential private random forest. In *Proceedings of the 2014 International Conference on Advances in Computing, Communications and Informatics, ICACCI 2014*, pages 2623–2630. IEEE, 2014.
- F. Pedregosa, G. Varoquaux, A. Gramfort, V. Michel, B. Thirion, O. Grisel, M. Blondel, P. Prettenhofer, R. Weiss, V. Dubourg, J. Vanderplas, A. Passos, D. Cournapeau, M. Brucher, M. Perrot, and E. Duchesnay. Scikit-learn: Machine learning in Python. *Journal of Machine Learning Research*, 12:2825–2830, 2011.
- Laurent Perron and Frédéric Didier. Cp-sat, 2024. URL https://developers.google.com/optimization/cp/cp_solver/.
- Le Trieu Phong, Yoshinori Aono, Takuya Hayashi, Lihua Wang, and Shiho Moriai. Privacy-preserving deep learning: Revisited and enhanced. In *Applications and Techniques in Information Security - 8th International Conference, ATIS 2017*, volume 719 of *Communications in Computer and Information Science*, pages 100–110. Springer, 2017.
- Santu Rana, Sunil Kumar Gupta, and Svetha Venkatesh. Differentially private random forest with high utility. In *IEEE International Conference on Data Mining, ICDM 2015*, pages 955–960, 2015.
- Maria Rigaki and Sebastian Garcia. A survey of privacy attacks in machine learning. *ACM Computing Surveys*, 56(4):1–34, November 2023. ISSN 1557-7341.
- Ahmed Salem, Apratim Bhattacharya, Michael Backes, Mario Fritz, and Yang Zhang. Updates-leak: Data set inference and reconstruction attacks in online learning. In *29th USENIX Security Symposium, USENIX Security 2020*, pages 1291–1308. USENIX Association, 2020.
- Pierre Stock, Igor Shilov, Ilya Mironov, and Alexandre Sablayrolles. Defending against reconstruction attacks with rényi differential privacy. *CoRR*, abs/2202.07623, 2022.
- Dayong Ye, Sheng Shen, Tianqing Zhu, Bo Liu, and Wanlei Zhou. One parameter defense - defending against data inference attacks via differential privacy. *IEEE Trans. Inf. Forensics Secur.*, 17:1466–1480, 2022.
- I-Cheng Yeh and Che hui Lien. The comparisons of data mining techniques for the predictive accuracy of probability of default of credit card clients. *Expert Systems with Applications*, 36(2, Part 1):2473–2480, 2009. ISSN 0957-4174.
- Alexander Ziller, Tamara T Mueller, Simon Stieger, Leonhard F Feiner, Johannes Brandt, Rickmer Braren, Daniel Rueckert, and Georgios Kaissis. Reconciling privacy and accuracy in ai for medical imaging. *Nature Machine Intelligence*, pages 1–11, 2024.

A Reconstruction Attack when N is Unknown

A.1 Confidence Interval on N

While reconstruction attacks targeting a complete dataset recovery in the literature generally assume knowledge of its size N [Dwork et al., 2017], our approach can be slightly adapted to be applicable without this information. In this section, we provide and empirically evaluate a CP formulation derived from the one presented in Section 3 that does not rely on knowing N . While this setup is both more generic and more realistic, it is also more challenging.

When N is unknown, it becomes a variable to infer. To bound the search, we will first calculate a confidence interval $[[N_{\text{MIN}}, N_{\text{MAX}}]]$. According to the DP RF algorithm in Section 2.2, each training example is used exactly once per tree. Thus, for a tree $t \in \mathcal{T}$, the sum of the non-noisy leaves' counts equals N . In our case, since the Laplace noise is centered at zero, for a tree $t \in \mathcal{T}$, we can expect the sum $N_t^* = \sum_{v,c} n_{tvc}^*$ to lie close to N .

We know that the noisy counts are computed by the Laplace mechanism as follows:

$$n_{tvc}^* = \text{int}(n_{tvc} + Y_{tvc}) = n_{tvc} + \text{int}(Y_{tvc}),$$

in which Y_{tvc} is a random variable sampled from a Laplace distribution $\text{Lap}(1/\varepsilon_v)$ and $\text{int}(\cdot)$ is the integer part function. Recall that the per-tree DP budget ε_v is computed by dividing the total privacy budget among the trees: $\varepsilon_v = \varepsilon/|\mathcal{T}|$. The variance of each Y_{tvc} is $\text{Var}(Y_{tvc}) = 2/\varepsilon_v^2$. Since the Y_{tvc} random variables are i.i.d., the variance of their sum ζ_t (whose N_t^* is a realization) is:

$$\text{Var}(\zeta_t) = \text{Var}\left(\sum_{v \in \mathcal{V}_t^L} \sum_{c \in \mathcal{C}} Y_{tvc}\right) = \sum_{v \in \mathcal{V}_t^L} \sum_{c \in \mathcal{C}} \text{Var}(Y_{tvc}) = |\mathcal{V}_t^L| \cdot |\mathcal{C}| \cdot \frac{2}{\varepsilon_v^2},$$

with a standard deviation:

$$\sigma_{N_t^*} = \frac{\sqrt{2 \cdot |\mathcal{V}_t^L| \cdot |\mathcal{C}|}}{\varepsilon_v}.$$

Let $N^* = \frac{1}{|\mathcal{T}|} \sum_{t \in \mathcal{T}} N_t^*$ be the average noisy count across all trees. By the Central Limit Theorem, N^* approximately follows a normal distribution for large $|\mathcal{T}|$. Thus, the 95% confidence interval $[[N_{\text{MIN}}, N_{\text{MAX}}]]$ can be defined as:

$$N_{\text{MAX}} = N^* + t_{95} \frac{\sigma_{\zeta_t}}{\sqrt{|\mathcal{T}|}} \quad \text{and} \quad N_{\text{MIN}} = \max\left(1, N^* - t_{95} \frac{\sigma_{\zeta_t}}{\sqrt{|\mathcal{T}|}}\right),$$

in which t_{95} is the Student's t-coefficient for a 95% confidence level according to $|\mathcal{T}|$.

A.2 Adapted Constraint Programming Formulation

As in the formulation presented in Section 3, for each leaf $v \in \mathcal{V}_t^L$ of each tree $t \in \mathcal{T}$, we let variables $n_{tvc} \in \{\max(0, n_{tvc}^* - \delta), \dots, n_{tvc}^* + \delta\}$ and $\Delta_{tvc} \in \{-\delta, \dots, \delta\}$ respectively model the (guessed) number of examples of class c within this leaf and the amount of noise added to it. We also use variable $\tilde{N} \in \{N_{\text{MIN}}, \dots, N_{\text{MAX}}\}$ to encode the (guessed) number of reconstructed examples.

Since N is unknown, we define variables for up to N_{MAX} examples in the worst-case. For each example $k \in \{1, \dots, N_{\text{MAX}}\}$, $x_{ki} \in \{0, 1\}$ represents the value of its attribute $i \in \{1, \dots, M\}$ in the reconstruction, while $z_{kc} \in \{0, 1\}$ equals 1 if and only if it belongs to class c . Although these reconstruction variables are defined for N_{MAX} examples, the attack's output is obtained from the first \tilde{N} examples.

Finally, we define a set of variables modelling the path of each example $k \in \{1, \dots, N_{\text{MAX}}\}$ through each tree $t \in \mathcal{T}$: variable $y_{tvkc} \in \{0, 1\}$ indicates if it is classified in class $c \in \mathcal{C}$ by leaf $v \in \mathcal{V}_t^L$. Given these variables, as previously, we define constraints to compute class counts and connect them

to the assignments of examples to leaves:

$$\sum_{v \in \mathcal{V}_t^L} \sum_{c \in \mathcal{C}} n_{tvc} = \tilde{N} \quad t \in \mathcal{T} \quad (10)$$

$$\sum_{c \in \mathcal{C}} z_{kc} = 1 \quad k \in \{1, \dots, N_{\text{MAX}}\} \quad (11)$$

$$z_{kc} = 0 \Rightarrow \sum_{t \in \mathcal{T}} \sum_{v \in \mathcal{V}_t^L} y_{tvkc} = 0 \quad k \in \{1, \dots, N_{\text{MAX}}\}, c \in \mathcal{C} \quad (12)$$

$$k > \tilde{N} \Rightarrow \sum_{t \in \mathcal{T}} \sum_{v \in \mathcal{V}_t^L} \sum_{c \in \mathcal{C}} y_{tvkc} = 0 \quad k \in \{1, \dots, N_{\text{MAX}}\} \quad (13)$$

$$\sum_{k=1}^{N_{\text{MAX}}} y_{tvkc} = n_{tvc} \quad t \in \mathcal{T}, v \in \mathcal{V}_t^L, c \in \mathcal{C} \quad (14)$$

Constraint (10) ensures that the examples' counts sum up to \tilde{N} within each tree. Constraint (11) guarantees that each example is associated with exactly one class. Constraint (12) enforces that each example can only contribute to the counts of its class. Note that this constraint differs from the formulation presented in Section 3. Indeed, if $z_{kc} = 1$ but $k > \tilde{N}$, example k is actually not part of the reconstructed dataset and hence is not assigned to any leaf of any tree, as stated in Constraint (13). Constraint (14) ensures consistency between the examples' assignments to the leaves and the (guessed) counts.

Finally, the rest of the model remains unchanged, the following constraint enforces consistency between the examples' assignments to the leaves, and the value of their attributes:

$$\sum_{c \in \mathcal{C}} y_{tvkc} = 1 \Rightarrow \left(\bigwedge_{i \in \Phi_v^+} x_{ki} = 1 \right) \wedge \left(\bigwedge_{i \in \Phi_v^-} x_{ki} = 0 \right) \quad t \in \mathcal{T}, v \in \mathcal{V}_t^L, k \in \{1, \dots, N_{\text{MAX}}\}, \quad (15)$$

The original objective is also retained with $\Delta_{tvc} = n_{tvc}^* - n_{tvc}$:

$$\max \sum_{t \in \mathcal{T}} \sum_{v \in \mathcal{V}_t^L} \sum_{c \in \mathcal{C}} \sum_{l=-\delta}^{\delta} \log(p_l) \mathbb{1}_{\Delta_{tvc}=l}. \quad (16)$$

A.3 Experimental Evaluation

To assess the effectiveness of our reconstruction attack in a context where the number of training examples N is unknown, we reproduce the experimental setup as described in Section 4.1, using our modified attack formulation introduced in the previous subsection. The computation of the reconstruction error must be slightly adapted. Indeed when N is known, the attack's performance is assessed by determining the correspondence between reconstructed and original examples using a minimum-cost matching. The average distance between these matched pairs defines the reconstruction error. However, when N is unknown, it is possible that the inferred reconstruction contains more (or less) than N examples, making this pairwise matching not directly applicable. In the case in which the number of reconstructed examples exceeds the actual one ($\tilde{N} > N$), we randomly duplicate some (true) training examples. In contrast, if the number of reconstructed examples is smaller than the actual one ($\tilde{N} < N$), we randomly subsample the same number of examples from the original training set. The same minimum-cost matching is then performed and the average distance between pairs of matched examples defines the reconstruction error.

The results of these experiments are presented in Table 2 for all datasets, forest sizes $|\mathcal{T}|$ and tree depths d . Comparing these results with those in Table 1 reveals two key trends. First, a few more runs failed to retrieve a feasible reconstruction within the given time frame (2 hours), indicating that the attack is computationally more expensive in this setup. This is expected, as the modified CP model introduces additional variables and constraints, leading to a larger search space and calling for longer solution times. Still, in most cases, the attack finds a feasible reconstruction. Second, and more importantly, the reconstruction error remains comparable to the case in which N is known. Despite the increased computational cost, the attack is still able to retrieve meaningful information encoded by the forest regarding its training data in most cases, thereby confirming our **Result 5**.

Table 2: Experimental results without assuming the training set size N is known. The table reports the average reconstruction error across varying numbers of trees $|\mathcal{T}|$, tree depths d and privacy budgets ε for the three datasets. The cases for which the solver did not find a feasible reconstruction within the 2-hour time limit are indicated by “-”.

		Adult			COMPAS			Default Credit		
		$d = 3$	$d = 5$	$d = 7$	$d = 3$	$d = 5$	$d = 7$	$d = 3$	$d = 5$	$d = 7$
$ \mathcal{T} = 1$	$\varepsilon = 0.1$	0.26	0.24	0.20	0.27	0.24	0.16	0.34	0.31	0.26
	$\varepsilon = 1$	0.26	0.24	0.17	0.26	0.22	0.15	0.34	0.30	0.22
	$\varepsilon = 5$	0.25	0.15	0.22	0.25	0.28	0.22	0.32	0.31	0.27
	$\varepsilon = 10$	0.25	0.13	0.24	0.25	0.20	0.20	0.32	0.29	0.30
	$\varepsilon = 20$	0.25	0.13	0.28	0.25	0.19	0.19	0.32	0.28	0.28
	$\varepsilon = 30$	0.25	0.12	0.28	0.25	0.20	0.20	0.32	0.30	0.15
$ \mathcal{T} = 5$	$\varepsilon = 0.1$	0.24	0.24	0.26	0.23	0.20	0.33	0.30	0.25	0.44
	$\varepsilon = 1$	0.19	0.24	0.20	0.15	0.20	0.14	0.24	0.23	0.23
	$\varepsilon = 5$	0.17	0.15	0.25	0.10	0.08	0.08	0.22	0.17	0.18
	$\varepsilon = 10$	0.17	0.13	0.11	0.10	0.06	0.05	0.22	0.15	0.14
	$\varepsilon = 20$	0.16	0.13	0.09	0.10	0.07	0.03	0.21	0.16	0.12
	$\varepsilon = 30$	0.16	0.12	0.09	0.10	0.06	0.03	0.21	0.17	0.12
$ \mathcal{T} = 10$	$\varepsilon = 0.1$	0.28	0.31	0.56	0.26	0.24	-	0.32	0.31	0.47
	$\varepsilon = 1$	0.24	0.35	0.25	0.24	0.20	0.18	0.28	0.29	0.26
	$\varepsilon = 5$	0.14	0.15	0.19	0.10	0.09	0.09	0.16	0.19	0.21
	$\varepsilon = 10$	0.13	0.12	0.15	0.07	0.06	0.07	0.14	0.16	0.17
	$\varepsilon = 20$	0.12	0.10	0.11	0.06	0.03	0.04	0.14	0.13	0.13
	$\varepsilon = 30$	0.12	0.09	0.09	0.06	0.03	0.03	0.14	0.12	0.11
$ \mathcal{T} = 20$	$\varepsilon = 0.1$	0.30	0.49	-	0.29	0.38	-	0.33	0.49	-
	$\varepsilon = 1$	0.31	0.26	0.48	0.33	0.26	0.28	0.30	0.29	0.49
	$\varepsilon = 5$	0.15	0.20	0.29	0.14	0.19	0.20	0.18	0.22	0.35
	$\varepsilon = 10$	0.12	0.15	0.20	0.08	0.08	0.11	0.15	0.18	0.23
	$\varepsilon = 20$	0.10	0.12	0.15	0.07	0.06	0.09	0.13	0.15	0.19
	$\varepsilon = 30$	0.10	0.10	0.12	0.06	0.05	0.07	0.13	0.13	0.15
$ \mathcal{T} = 30$	$\varepsilon = 0.1$	0.38	0.35	-	0.37	0.29	-	0.37	0.49	-
	$\varepsilon = 1$	0.38	0.27	0.53	0.38	0.28	0.32	0.34	0.30	0.48
	$\varepsilon = 5$	0.19	0.26	0.25	0.17	0.27	0.23	0.21	0.27	0.30
	$\varepsilon = 10$	0.13	0.15	0.32	0.09	0.10	0.18	0.18	0.19	0.28
	$\varepsilon = 20$	0.11	0.12	0.21	0.08	0.08	0.10	0.15	0.14	0.24
	$\varepsilon = 30$	0.10	0.11	0.19	0.07	0.07	0.09	0.14	0.13	0.21

B Determining a Search Interval for Noise Values

Rather than modelling all possible (integer) random noise values Y_{tvc} within \mathbb{Z} , our CP model focuses on a (sufficient) predefined range $\{-\delta, \dots, \delta\}$ such that $\mathbb{P}(\text{int}(Y_{tvc}) \in \{-\delta, \dots, \delta\}) \geq 0.999$. In practice, we use $\delta = \lceil 12/\varepsilon_v \rceil$. As displayed in Figure 5, this value is suitable for all considered privacy budgets ε_v . Indeed, it always leads to the definition of slightly wider search intervals for the variables modelling the noise, theoretically guaranteeing that the probability of the actual noise value being within it is greater than 0.999.

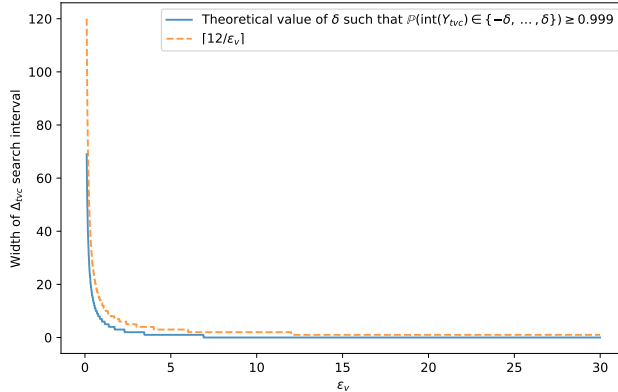


Figure 5: Width of Δ_{tvc} search interval as a function of ε_v . As expected, the magnitude of the noise added decreases when the privacy budget increases, resulting in a smaller search interval.

C Additional Experimental Results

C.1 Running Times

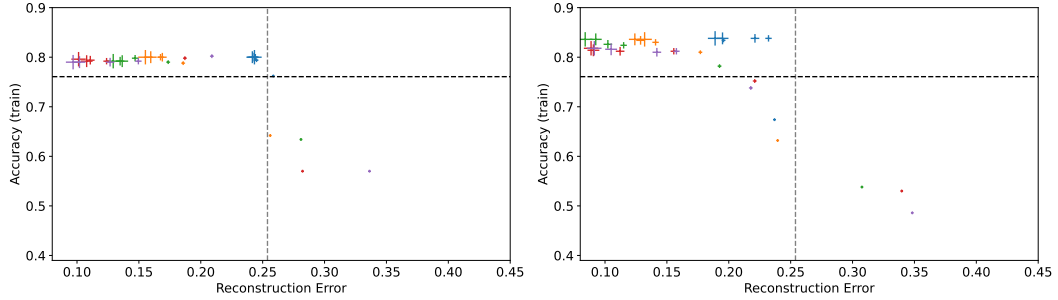
The average running time (over all performed experiments) to find a feasible reconstruction is below two minutes. Table 3 details the running time required by the CP solver to find a feasible reconstruction, averaged over the 5 random seeds for all considered datasets, numbers of trees $|\mathcal{T}|$ within the target forest, tree depths d and privacy budgets ε . Several general trends can be observed. Increasing the number of trees or their depth leads to larger CP models, including more variables, more constraints and larger search spaces. This logically increases the solver’s running time. Considering tight privacy budgets also widens the solver’s search space and running time. Nevertheless, in all cases, the CP solver is able to find a feasible reconstruction using only a fraction of its predefined 2-hours timeout, and can then use the remaining time to refine it and improve its objective function (corresponding to the noise likelihood, as explained in Section 3).

C.2 Trade-offs between Predictive Performance and Reconstruction Error

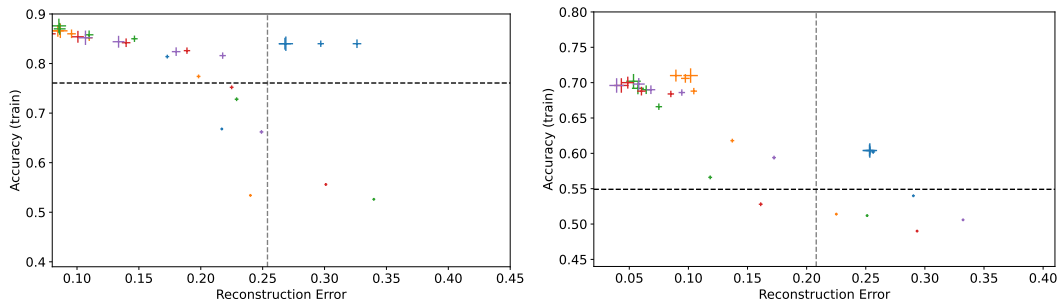
Figures 6 and 7 present the detailed trade-offs between the RFs’ predictive performance and the empirical reconstruction error of our attack across all experiments. These figures confirm the key trends discussed in the main paper (in particular **Result 3**), and are consistent across all datasets, privacy budgets, tree depths and forest sizes. In particular, most RFs are located either in the top-left or bottom-right corners of the plots. The top-left region corresponds to RFs with non-trivial predictive performance, giving some advantage to the reconstruction attack compared to the random baseline, while the bottom-right region includes RFs that provide no significant advantage for the reconstruction attack but perform worse than a majority classifier. Interestingly, the few RFs that exhibit non-trivial predictive performance while remaining resilient to reconstruction attacks (top-right corner) are also the sparsest, mostly consisting of a single tree ($|\mathcal{T}| = 1$). This suggests that information from multiple trees can typically be aggregated, substantially enhancing reconstruction attack success.

Table 3: Average running time (s) to get a feasible reconstruction for different numbers of trees $|\mathcal{T}|$ within the target forest, tree depths d and privacy budgets ε for the three datasets. The situation in which the solver failed to find a feasible reconstruction within the 2-hour time limit are marked with “-”.

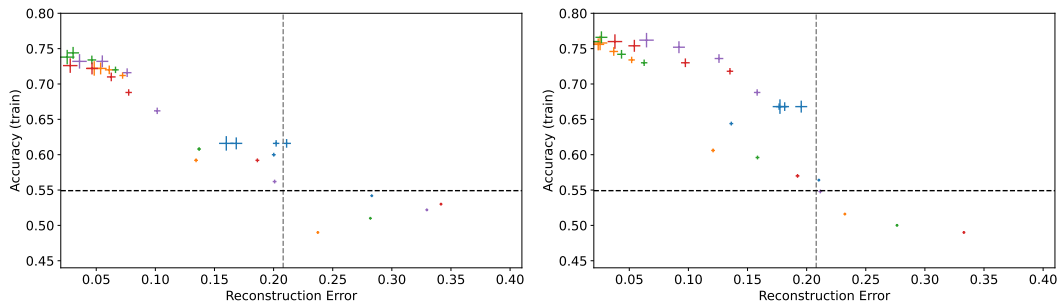
		Adult			COMPAS			Default Credit		
		$d = 3$	$d = 5$	$d = 7$	$d = 3$	$d = 5$	$d = 7$	$d = 3$	$d = 5$	$d = 7$
$ \mathcal{T} = 1$	$\varepsilon = 0.1$	1.81	9.73	24.98	1.95	7.10	22.77	2.65	9.48	28.37
	$\varepsilon = 1$	0.56	3.90	16.57	0.51	2.75	10.68	0.56	3.63	15.53
	$\varepsilon = 5$	0.45	3.15	13.57	0.49	2.61	9.89	0.53	3.60	14.84
	$\varepsilon = 10$	0.47	3.16	13.78	0.47	2.65	10.03	0.51	3.69	16.69
	$\varepsilon = 20$	0.46	1.95	13.35	0.39	2.26	9.66	0.37	1.65	12.21
	$\varepsilon = 30$	0.41	1.57	12.69	0.43	2.50	9.74	0.48	2.78	15.54
$ \mathcal{T} = 5$	$\varepsilon = 0.1$	14.35	47.58	123.09	10.41	39.33	96.10	12.94	41.43	128.34
	$\varepsilon = 1$	6.61	22.23	60.73	4.84	24.05	67.07	4.52	23.36	56.40
	$\varepsilon = 5$	3.72	23.87	53.88	3.72	25.14	71.13	3.56	28.15	79.50
	$\varepsilon = 10$	4.23	26.25	75.20	3.82	22.80	73.11	3.00	24.55	88.45
	$\varepsilon = 20$	2.95	24.62	85.41	3.32	20.51	63.55	3.82	22.55	54.54
	$\varepsilon = 30$	2.68	24.47	110.77	3.60	27.20	51.81	3.27	22.18	118.82
$ \mathcal{T} = 10$	$\varepsilon = 0.1$	34.90	94.27	284.07	27.20	75.29	422.43	31.08	108.73	442.63
	$\varepsilon = 1$	17.79	42.57	157.09	18.73	45.19	103.73	14.70	48.83	109.73
	$\varepsilon = 5$	10.88	43.60	93.64	9.19	41.73	83.29	12.10	44.93	97.78
	$\varepsilon = 10$	10.88	47.81	98.43	10.72	44.00	125.38	12.11	100.56	122.64
	$\varepsilon = 20$	10.35	40.89	106.39	8.62	39.82	119.52	12.33	63.34	124.82
	$\varepsilon = 30$	8.68	46.77	90.21	12.32	46.17	87.92	9.17	41.91	284.96
$ \mathcal{T} = 20$	$\varepsilon = 0.1$	90.69	293.24	1033.74	84.66	282.49	968.48	97.05	261.93	1022.18
	$\varepsilon = 1$	32.68	92.48	357.22	26.43	89.08	300.26	30.97	85.97	354.49
	$\varepsilon = 5$	22.18	65.19	167.35	22.18	68.28	206.02	17.92	66.48	225.78
	$\varepsilon = 10$	22.39	68.52	234.35	27.08	67.73	254.61	19.43	71.50	242.74
	$\varepsilon = 20$	28.65	225.42	360.96	25.57	125.94	279.20	21.58	243.11	890.48
	$\varepsilon = 30$	35.18	233.34	387.37	26.55	72.33	285.36	25.58	127.86	511.48
$ \mathcal{T} = 30$	$\varepsilon = 0.1$	185.31	842.61	-	170.20	699.23	-	150.73	752.15	-
	$\varepsilon = 1$	47.45	152.51	611.71	39.69	146.58	666.69	41.66	158.16	451.77
	$\varepsilon = 5$	29.43	101.53	405.87	26.72	95.50	259.35	31.40	89.66	438.50
	$\varepsilon = 10$	31.83	92.64	363.51	28.17	86.97	333.50	30.04	96.03	380.74
	$\varepsilon = 20$	34.24	87.08	357.17	58.27	212.95	375.59	32.66	119.71	413.38
	$\varepsilon = 30$	45.91	410.98	536.70	32.32	217.46	828.98	36.58	232.30	862.32



(a) UCI Adult Income dataset, depth 3 decision trees. (b) UCI Adult Income dataset, depth 5 decision trees.



(c) UCI Adult Income dataset, depth 7 decision trees. (d) COMPAS dataset, depth 3 decision trees.



(e) COMPAS dataset, depth 5 decision trees. (f) COMPAS dataset, depth 7 decision trees.

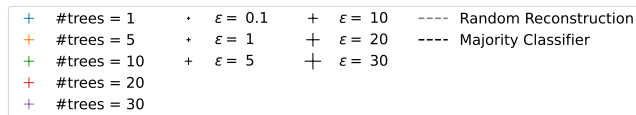
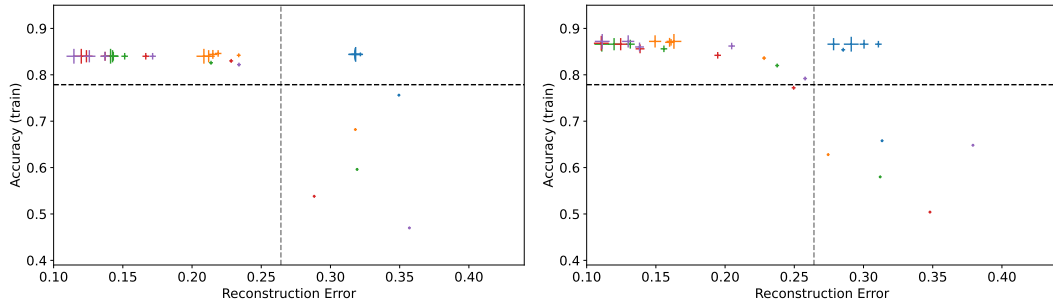
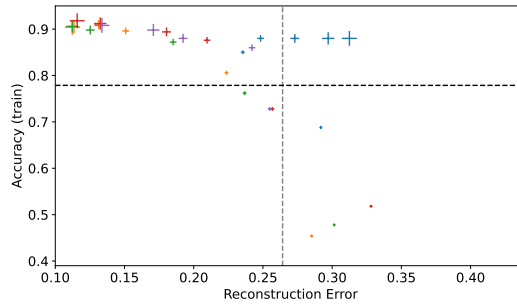


Figure 6: Average training accuracy of ϵ -DP RFs as a function of the reconstruction error of our attack for different numbers of trees $|\mathcal{T}|$ and privacy budgets ϵ , for the considered datasets and tree depths values.



(a) Default Credit dataset, depth 3 decision trees.

(b) Default Credit dataset, depth 5 decision trees.



(c) Default Credit dataset, depth 7 decision trees.

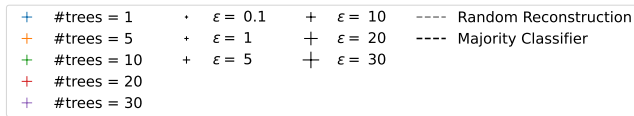


Figure 7: Average training accuracy of ϵ -DP RFs as a function of the reconstruction error of our attack for different numbers of trees $|\mathcal{T}|$ and privacy budgets ϵ , for the considered datasets and tree depths values (continued).

D Privacy Leak Analysis

As discussed in Section 4.2, our proposed reconstruction attack is often able to generate reconstructed datasets that are closer to the actual RF training set D than a random baseline uniformly sampling the attributes’ values within their respective domains. While this suggests that the RFs provide information regarding D even with thorough DP guarantees, this information can either be distribution-wide or specific to D . While the former case can still be problematic if the entity owning the data does not want to leak its distribution, it arguably does not correspond to a *privacy leak*, which occurs if information specific to the actual RF training set D can be retrieved [Cohen et al., 2025]. In this appendix, we aim at quantifying the later, by investigating whether the reconstructed dataset is closer to D than to other datasets drawn from the same distribution in a statistically significant manner.

More precisely, for each performed experiment, we compute the error (i) between the reconstructed dataset and the actual RF training dataset (as reported in Section 4.2) and (ii) between the reconstructed dataset and datasets of the same size sampled from the same distribution. Intuitively, any decrease in the measurement (i) compared to (ii) is an indication that the attack is able to retrieve information specific to the particular individuals belonging to the RF training set, rather than solely general information about the data distribution. In such a case, a privacy leak can be identified, since, while an ML model may reasonably leak distributional information, it should not encode specific information about individual members of its training set.

In practice, we randomly sample 100 datasets containing N examples from the same distribution as D , and compute the errors between each of them and the reconstructed dataset. We then fit a normal distribution from this list of errors, estimating how likely it is to measure a given reconstruction error for a dataset randomly drawn from the data distribution. We finally compute the cumulative density function (CDF) of this fitted distribution for the actual reconstruction error, which quantifies *the likelihood of observing a reconstruction error lower or equal to the one measured on the actual RF training set, using a dataset randomly drawn from the same data distribution*. Hence, it is somewhat analogous to a p -value, with very small values corresponding to observations that are unlikely to be observed purely by chance. We illustrate this process on Figure 8 for a representative setup using DP RFs built of $|\mathcal{T}| = 10$ trees of depth 5, on the UCI Adult Income dataset. As it can be seen, the normal laws fit the distribution of the measured errors very well. More precisely, we report results for three particular experiments, using very tight $\epsilon = 0.1$ (Figure 8a), tight $\epsilon = 1$ (Figure 8b) or large $\epsilon = 30$ (Figure 8c) privacy budgets.

In the first case ($\epsilon = 0.1$), the results previously presented in Table 1 show that the reconstruction is not more accurate than the random baseline. Thus, no information is retrieved from the trained RF. Unsurprisingly, the reconstructed dataset is as far from datasets randomly drawn from the data distribution as it is from the actual RF training dataset. However in the two other situations, we observed in Table 1 a significant decrease of the reconstruction error compared to the random baseline: for $\epsilon = 1$ and $\epsilon = 30$, useful information is extracted from the trained RF. For $\epsilon = 1$, Figure 8b suggests that this information is mainly distributional: the reconstructed dataset is not significantly closer to the actual RF training dataset than it is from other datasets from the same distribution. Formally, there is a non-negligible 11.4% chance that a dataset randomly drawn from the data distribution is closer to the reconstructed dataset than the actual RF training set. In turn, for $\epsilon = 30$, the inferred information can be considered as a privacy leak. Indeed, as evidenced in Figure 8c, there is a negligible probability (10^{-7}) that the actual RF training set lies as close to the reconstructed dataset by chance (given the data distribution).

We report the average results (estimated CDF) of all experiments in Table 4. They suggest that a privacy leak is *likely* (CDF for the training set reconstruction error $\leq 5\%$) for most configurations using privacy budget $\epsilon \geq 5$. Importantly, even for tighter privacy budgets (e.g., $\epsilon = 1$), the results for some configurations still suggest possible privacy leaks, highlighting the importance of the choice of hyperparameters and their influence over the privacy-accuracy trade-off. It is worth noting that several configurations yield CDF values slightly above 5% but remaining reasonably low – which suggests that the reconstructed dataset is closer from the actual RF training set than from average datasets randomly sampled from the same distribution, potentially indicating a moderate privacy leak.

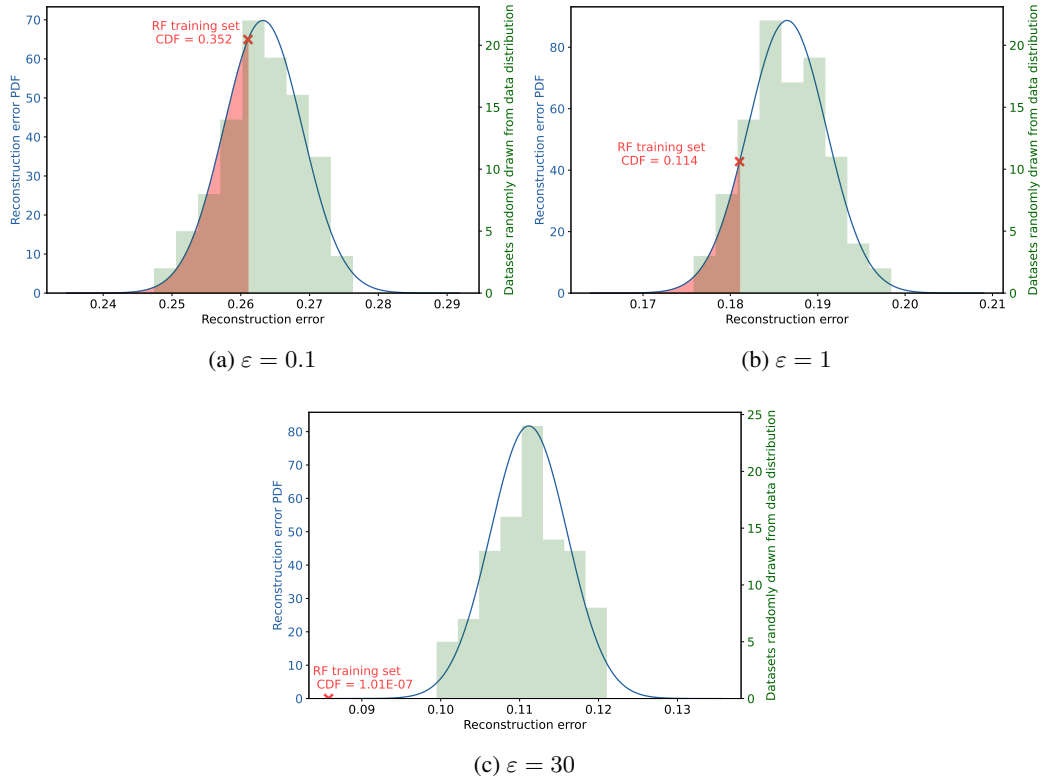


Figure 8: Distribution of the errors measured between the reconstructed dataset and datasets randomly drawn from the data distribution. We report the actual proportions in green, and the fitted distribution (probability density function – PDF) in blue. We then compute the cumulative density function (CDF) at the point corresponding to the reconstruction error measured using the actual RF training dataset. This value quantifies *how likely it is to observe a reconstruction error lower or equal to the one measured on the actual RF training set, using a dataset randomly drawn from the same data distribution*. We display this process for the experiments on the UCI Adult Income dataset, using $|\mathcal{T}| = 10$ trees of depth 5, with three distinct DP budgets ε (for a given random seed).

Table 4: Privacy leak quantification: the reported values quantify *the likelihood of observing a reconstruction error lower or equal to the one measured on the actual RF training set, using a dataset randomly drawn from the same data distribution*. More precisely, we first estimate the distribution of the errors measured between the dataset reconstructed from the trained RF and datasets randomly drawn from the data distribution. Then, we compute and report in this table the cumulative density function (CDF) at the point corresponding to the reconstruction error measured using the actual RF training dataset. We display it for different numbers of trees $|\mathcal{T}|$ within the target forest, tree depths d and privacy budgets ε for the three datasets. The situations in which the solver failed to find a feasible reconstruction within the 2-hour time limit are marked with “-”. Values below 5% are **bold**, indicating that there is a very small-to-negligible probability that the actual RF training set lies as close to the reconstructed dataset by chance (given the data distribution).

	Adult			COMPAS			Default Credit			
	$d = 3$	$d = 5$	$d = 7$	$d = 3$	$d = 5$	$d = 7$	$d = 3$	$d = 5$	$d = 7$	
$ \mathcal{T} = 1$	$\varepsilon = 0.1$	0.208	0.544	0.344	0.614	0.480	0.464	0.852	0.884	0.914
	$\varepsilon = 1$	0.106	0.225	0.144	0.528	0.357	0.212	0.803	0.771	0.535
	$\varepsilon = 5$	0.074	0.277	0.067	0.464	0.271	0.102	0.764	0.613	0.146
	$\varepsilon = 10$	0.072	0.229	0.147	0.461	0.274	0.158	0.761	0.622	0.211
	$\varepsilon = 20$	0.072	0.205	0.201	0.454	0.328	0.262	0.761	0.762	0.081
	$\varepsilon = 30$	0.071	0.205	0.172	0.461	0.254	0.286	0.762	0.790	0.074
$ \mathcal{T} = 5$	$\varepsilon = 0.1$	0.164	0.308	0.264	0.358	0.342	0.177	0.823	0.748	0.778
	$\varepsilon = 1$	0.087	0.266	0.079	0.331	0.042	0.208	0.644	0.534	0.651
	$\varepsilon = 5$	0.035	0.061	0.002	0.114	3.01E-05	3.37E-05	0.606	0.034	0.027
	$\varepsilon = 10$	0.053	0.007	1.14E-04	0.023	9.09E-07	5.01E-08	0.618	0.033	1.77E-04
	$\varepsilon = 20$	0.008	0.007	8.75E-06	0.035	5.66E-08	1.16E-11	0.715	0.002	1.98E-05
	$\varepsilon = 30$	0.008	0.011	8.03E-07	0.022	2.52E-07	1.60E-10	0.685	0.002	4.24E-04
$ \mathcal{T} = 10$	$\varepsilon = 0.1$	0.304	0.332	0.321	0.326	0.512	0.101	0.652	0.438	0.446
	$\varepsilon = 1$	0.066	0.144	0.021	0.030	0.190	0.127	0.442	0.543	0.463
	$\varepsilon = 5$	0.077	0.001	0.003	0.022	0.001	2.74E-04	0.297	0.068	0.087
	$\varepsilon = 10$	0.031	0.001	1.31E-04	0.002	5.08E-06	4.65E-05	0.149	0.011	7.00E-06
	$\varepsilon = 20$	0.039	9.42E-04	1.80E-07	1.19E-04	5.59E-07	1.70E-11	0.173	1.46E-04	7.26E-04
	$\varepsilon = 30$	0.007	3.82E-07	1.92E-06	2.65E-05	4.89E-09	8.05E-13	0.200	8.57E-05	1.23E-08
$ \mathcal{T} = 20$	$\varepsilon = 0.1$	0.143	0.395	0.219	0.443	0.436	0.239	0.548	0.546	0.559
	$\varepsilon = 1$	0.176	0.132	0.093	0.233	0.372	0.342	0.379	0.540	0.571
	$\varepsilon = 5$	0.016	0.056	0.008	0.069	0.022	0.101	0.170	0.245	0.195
	$\varepsilon = 10$	0.009	0.006	8.69E-04	0.008	0.008	0.032	0.092	0.005	0.131
	$\varepsilon = 20$	0.021	2.84E-04	6.46E-06	1.66E-04	7.96E-05	6.69E-04	0.008	7.05E-04	0.004
	$\varepsilon = 30$	0.002	1.20E-05	6.32E-08	2.68E-05	5.86E-10	1.18E-07	0.004	8.61E-05	1.31E-05
$ \mathcal{T} = 30$	$\varepsilon = 0.1$	0.383	0.364	-	0.274	0.302	-	0.630	0.501	-
	$\varepsilon = 1$	0.179	0.069	0.064	0.309	0.389	0.271	0.461	0.452	0.453
	$\varepsilon = 5$	0.125	0.007	0.028	0.054	0.036	0.119	0.113	0.141	0.291
	$\varepsilon = 10$	0.064	0.004	0.008	0.050	0.001	0.107	0.017	0.001	0.071
	$\varepsilon = 20$	0.006	5.75E-04	0.001	0.001	1.07E-04	0.084	0.006	7.83E-04	0.032
	$\varepsilon = 30$	2.50E-04	2.86E-04	0.001	3.84E-06	1.09E-08	1.63E-04	4.84E-04	5.11E-05	5.08E-04

E Additional Experiments on Scalability

In this section, we investigate the effect of the DP RFs training set size on the effectiveness of our dataset reconstruction attack. More precisely, we focus on DP RFs built of $|\mathcal{T}| = 10$ trees of depth 5, with DP budget $\varepsilon = 5$. This configuration is representative of the experimental conditions presented in Section 4.1. We train such DP RFs with varying numbers of training examples $N \in \{25, 50, 100, 200, 300, 400, 500\}$. The remaining of the setup is as described in Section 4.1 (in particular, all results are averaged across 5 different random seeds), apart from the maximum CPU time which is increased to 5 hours.

Table 5 displays the predictive accuracy of the built DP RFs, along with the success of the associated reconstruction attacks. Note that the results for the configuration used in Section 4.2 (i.e., $N = 100$) are slightly better here because the CP formulations are often not solved to optimality and the solver benefits the additional running time to find slightly better solutions. This suggests that the results presented throughout the paper are likely to improve with increased adversarial computational power and advancements in CP solver technologies. We observe that as the training set size N increases, the test set accuracy of the built DP RFs improves significantly. Meanwhile, the training accuracy decreases and converges toward the test accuracy, indicating better generalization of the built DP RFs. Another interesting phenomenon can be observed: the DP RFs training and test set accuracies sometimes increase simultaneously while increasing the training set size N (e.g., from $N = 300$ to $N = 400$ for the Default Credit dataset). This is due to the fact that the relative impact of the added noise decreases when N increases, allowing for better predictive performances. Crucially, this reduction in the relative effect of noise over the trees' parameters also benefits the reconstruction attack: the reconstruction error significantly decreases as the size of the DP RF's training set N increases. For instance, while the reconstruction error from DP RFs trained on $N = 100$ examples from the UCI Adult Income dataset is 12.3% on average, this number decreases to 8.8% (hence a relative decrease of 28%) when it is trained on $N = 500$ examples, although the number of examples to retrieve is significantly greater.

Overall, these results suggest that the attack's performance is likely to improve as the size of the target DP RF training set increases, while also demonstrating the scalability of the proposed reconstruction approach.

Table 5: Results of our experiments on the reconstruction attack’s scalability. For varying training set sizes N , we report the predictive performances of the built DP RFs, along with the resulting reconstruction error (averaged over 5 different random seeds).

(a) UCI Adult Income dataset					(b) COMPAS dataset				
#Examples	Reconstruction error		RF Accuracy		#Examples	Reconstruction error		RF Accuracy	
	Avg	Std	Train	Test		Avg	Std	Train	Test
25	0.170	0.019	0.888	0.766	25	0.103	0.021	0.712	0.533
50	0.157	0.010	0.832	0.771	50	0.077	0.009	0.696	0.564
100	0.123	0.012	0.824	0.766	100	0.063	0.003	0.720	0.635
200	0.102	0.011	0.770	0.775	200	0.051	0.005	0.695	0.647
300	0.107	0.012	0.775	0.770	300	0.048	0.008	0.693	0.652
400	0.097	0.007	0.755	0.774	400	0.052	0.008	0.706	0.652
500	0.088	0.012	0.758	0.773	500	0.049	0.015	0.692	0.655

(c) Default of Credit Card Clients dataset				
#Examples	Reconstruction error		RF Accuracy	
	Avg	Std	Train	Test
25	0.229	0.017	0.920	0.772
50	0.182	0.015	0.876	0.780
100	0.158	0.016	0.856	0.782
200	0.139	0.012	0.828	0.782
300	0.125	0.007	0.827	0.782
400	0.129	0.011	0.828	0.786
500	0.114	0.007	0.814	0.787

F Additional Experiments on Partial Reconstruction

The purpose of this section is to determine whether (and to what extent) knowledge of part of the training set attributes (for all examples) helps reconstruct the others. As in the previous section, we focus on a representative setup with DP RFs built of $|\mathcal{T}| = 10$ trees of depth 5, with global DP budget $\varepsilon = 5$. For each dataset, we vary the number of known attributes between 0 and $M_o - 1$, in which M_o is the number of original (i.e., before one-hot encoding) features. Indeed, binary attributes one-hot encoding the same original feature are not independent from each other and considering them separately in this partial attributes knowledge setup would bias the reconstruction results. The number of such original features for the COMPAS (respectively, UCI Adult Income and Default Credit) dataset is 7 (respectively, 14 and 16). For each of the 5 random seeds, we randomly sample the $m \in \{0, \dots, M_o - 1\}$ known attributes. We then modify the CP formulation to fix the known attributes of each example to their true value, and solve the resulting CP model to retrieve the unknown ones.

We report in Figure 9 the reconstruction error (measured for the unknown attributes) as a function of the number of known attributes. The results for all three datasets consistently show that the knowledge of a number of attributes does not help reconstruct the others. The slight increase in reconstruction error when the number of known attributes increases can be explained by the alignment process: as explained in Section 4.1, to figure out which reconstructed example corresponds to which original one, we first perform a minimum cost matching, before computing the average reconstruction error for each pair of original-reconstructed examples. In this partial reconstruction setup, this matching is still performed on the complete examples’s features vector even though the attack only retrieves part

of their attributes. Hence, the improvement in reconstruction error induced by the matching process reduces as the number of unknown attributes decreases.

This observation empirically verifies the theoretical guarantees offered by DP: the protection enforced for the unknown attributes can not be “undone” through postprocessing the DP RF, even with the auxiliary information provided by the known attributes. In other words, DP prevents so-called *linkage attacks* [Dwork and Roth, 2014]. It is worth noting that these results contrast with the ones observed against non-DP RFs, for which knowledge of some of the attributes greatly helped reconstruct the others [Ferry et al., 2024b].

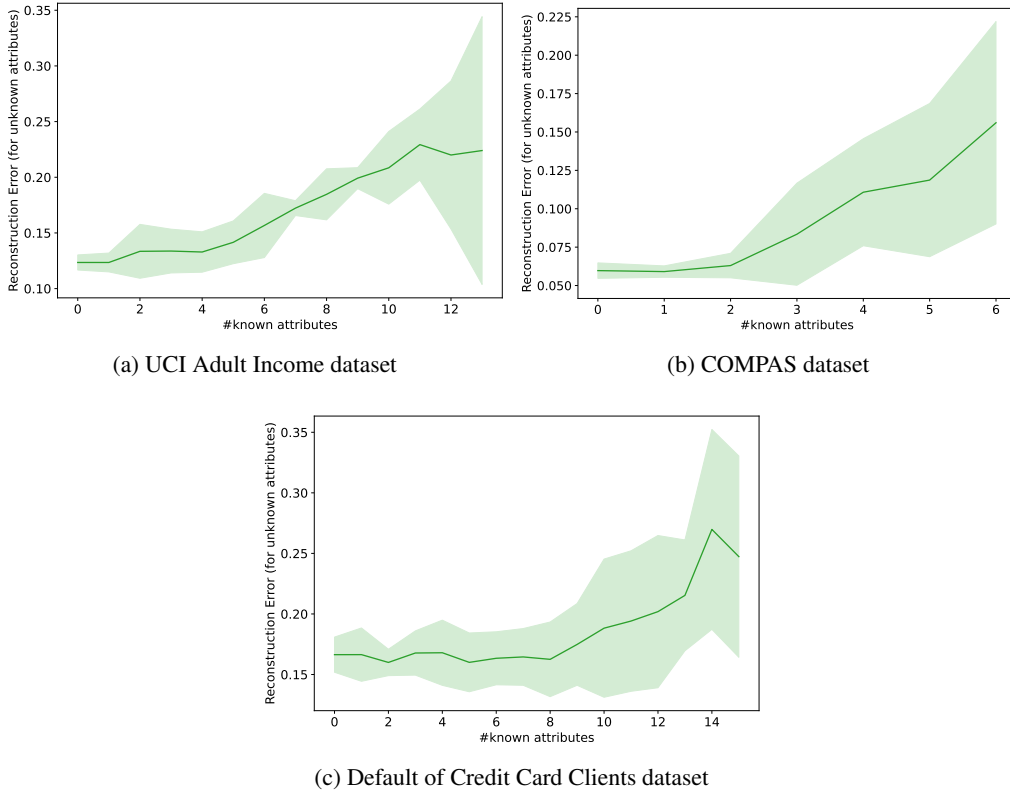


Figure 9: Results of reconstruction experiments with knowledge of some of the attributes. We report the reconstruction error (for the unknown attributes) as a function of the number of known attributes in the forest’s training set. For these experiments, all forests are built of $|\mathcal{T}| = 10$ trees of depth 5, with DP budget $\epsilon = 5$. Reconstruction errors are averaged over 5 different random seeds and we also report the standard deviation.

G Broader Impact Statement

Machine learning models are increasingly trained on sensitive private data, such as medical records or personal histories. The need to audit their decision-making processes (e.g., to prevent discriminatory practices) has led to regulations advocating for greater transparency. To enable the safe release of statistics, model predictions or trained models, DP has become a widely adopted standard due to its appealing theoretical properties.

However, DP does not (at least directly) provide theoretical protection against dataset reconstruction attacks. Our work demonstrates that, in practice, machine learning models can comply with rigorous DP guarantees while still leaking a significant portion of their training data. This critical finding highlights the need for developing new defense mechanisms, and emphasizes the importance of the design of the DP mechanism itself, beyond the sole privacy budget. Going in this direction, our study provides insights into the impact of different DP design choices and advocates for empirically evaluating a model’s resilience against a variety of reconstruction attacks—including the one

introduced in this work— before disclosure. Our findings emphasize that achieving privacy-preserving machine learning requires a holistic approach that carefully balances transparency, model utility, and empirical robustness against privacy threats. To this end, the proposed reconstruction attack provides a useful mathematically-rigorous way of benchmarking privacy protections.